

Ductility-Dip Cracking Susceptibility of Nickel-Based Weld Metals

Part 1: Strain-to-Fracture Testing

This investigation examines various factors including the threshold strain for cracking, transition to gross cracking, and effects of small compositional changes

BY N. E. NISSLEY AND J. C. LIPPOLD

ABSTRACT. In Part 1 of this investigation, the ductility-dip cracking (DDC) susceptibility of Ni-Cr-Fe filler metals was evaluated using the strain-to-fracture (STF) Gleeble-based testing technique. These high-chromium Ni-based filler metals are frequently used in nuclear power plant applications for welding Ni-based Alloy 690 and include filler metals 82, 52, and 52M (FM-82, FM-52, and FM-52M), a number of FM-52M-type experimental alloys including two with additions of molybdenum and niobium. The interpretation of the STF results includes both the threshold strain for cracking and the transition to gross cracking. In Part 2, an in-depth microstructural analysis of select alloys was conducted to add insight to the DDC mechanism.

The compositional changes in the FM-52M experimental alloys resulted in a range of DDC susceptibility, indicating the strong effect of minor changes in composition. A significant decrease in DDC susceptibility was observed in the experimental alloys with both Mo and Nb additions. The threshold strain for cracking in the 2.5% Nb and 4% Mo Ni-Cr-Fe alloy was approximately 8%, as compared to threshold values of approximately 1–3% for the other filler metals. The DDC resistance of the Mo and Nb modified filler metals was more than twice that observed in typical FM-82 alloys.

Introduction

Safety and life extension requirements in nuclear applications have driven the development of alloys with improved corrosion and elevated temperature properties. These new materials have, in turn, required the development of welding con-

sumables and joining techniques that meet or exceed the properties of the base materials.

In the 1950s, Ni-based Alloy 600 replaced 304 stainless steel in applications where resistance to stress corrosion cracking (SCC) was required (Ref. 1). Subsequent work to develop matching welding consumables led to the development of filler metal 82 (FM-82) (AWS A5.14 ERNiCr-3). Since then, Alloy 690 was developed with even better resistance to SCC and has replaced Alloy 600 for use in many nuclear steam generator components (Ref. 1). The first generation matching consumable for joining Alloy 690 was filler metal 52 (FM-52) (AWS A5.14 ERNiCrFe-7), which demonstrated better SCC and hot cracking resistance compared to FM-82 (Ref. 1). However, in highly restrained weldments, this filler metal was found to be susceptible to DDC (Refs. 2, 3). To overcome some of the problems encountered with FM-52, a second-generation consumable filler metal 52M (FM-52M) (AWS 5.14 ERNiCrFe-7A) (Ref. 1) was developed. It contained additions of B, Nb, and Zr to improve resistance to DDC and had reduced Al and Ti to reduce the tendency for floating oxide impurities.

Most of the DDC susceptible materials have a face-centered cubic and/or austenitic microstructure. They tend to be single phase from room temperature to melting and solidify as FCC. Ductility-dip cracking can occur along solidification or migrated grain boundaries (MGB) in weld metals of single-phase materials (Refs.

4–6). Migrated grain boundaries are the crystallographic portion of a solidification boundary that has moved or migrated from the compositional portion due to grain growth and grain boundary straightening (see Fig. 2.3) (Ref. 7). Materials with low impurity levels, no second phases, or precipitates have less resistance to MGB mobility and grain growth and as a result of this extra grain boundary mobility, these materials tend to have larger grains. Larger grain materials tend to be more susceptible to DDC than fine grain materials (Refs. 2, 3, 8–10); consequently, matching weld metals are typically more susceptible than wrought base materials (Refs. 3, 11). Lippold et al. (Ref. 12) proposed that this is a result of strain localization at grain boundaries, which increases with larger grained materials (less grain boundary area). Larger grains result in less boundary area for deformation mechanisms such as grain boundary sliding, which is considered to be a major element in DDC (Refs. 4, 5, 13). Under some conditions, second-phase precipitates have been reported to be effective in pinning migrated grain boundaries (Refs. 4, 14, 15) preventing grain growth and resulting in wavy boundaries. The grain boundary orientation relative to the applied stress was also found to be an important factor in the formation of DDC (Ref. 3) and has proven successful in reducing DDC in some applications.

Ductility-dip cracks are generally small, typically less than 3 mm long by 1 mm deep (Refs. 3, 16, 17). In high restraint weldments, however, they may be much larger. Liquation cracks and ductility-dip cracks often occur in the same weldment (Refs. 8, 18) and may be distinguished by fractographic examination employing scanning electron microscopy. Liquation cracks can be recognized by the evidence of liquid films along the fracture path while ductility-dip cracks show no evidence of liquation. However, not all liquation cracks exhibit clear evidence of liquid films; in such circumstances, they

KEYWORDS

Ductility-Dip Cracking (DDC)
Ni-Cr-Fe
Strain-to-Fracture (STF)
Alloy 690
Filler Metals 82, 52, and 52M
GTA Spot Weld

N. E. NISSLEY (nathannissley@gmail.com), formerly a graduate research associate at The Ohio State University, is currently with ExxonMobil Upstream Research Co., Houston, Tex. J. C. LIPPOLD is a professor in the Welding Engineering program at The Ohio State University.

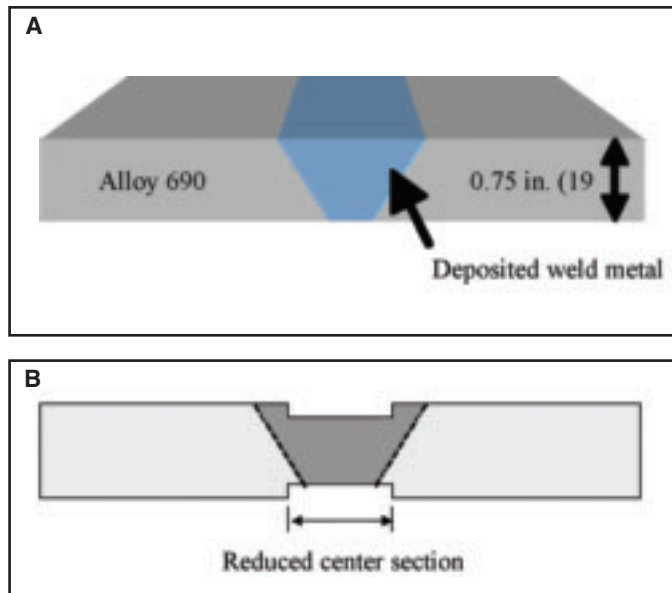
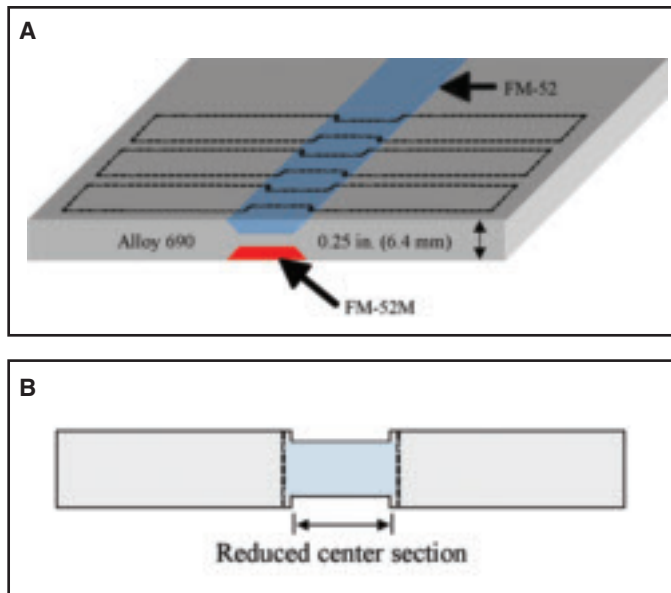


Fig. 1 — Sample preparation Method 1. A — Cross-sectional view of multipass welded plate with FM-52 and FM-52M filler metals. Strain-to-fracture sample blanks cut from the plate (dashed lines); B — face of the STF sample blank with reduced center section. The cross-hatched area indicates the location of the deposited weld metal with FM-52 on one side and the FM-52M on the other.

Fig. 2 — Sample preparation Method 2. A — Cross-sectional view of multipass welded plate with the different compositions tested. Sample had a single V-groove with a 60-deg included angle; B — face of the STF sample blank with reduced center section. The cross-hatched area indicates the location of the deposited weld metal.

can be confused with DDC unless detailed fractographic analysis is performed. Unequivocal evaluation and identification of DDC requires a test technique with sufficient control to avoid liquation cracking altogether.

Some of the most common test techniques used to evaluate DDC are the strain-to-fracture (STF) test (Ref. 19), the Transverse-Varestraint and Gleeble hot ductility tests (Ref. 2) and the spot-on-spot (double-spot) Varestraint test (Ref. 4). Several other tests are discussed elsewhere (Ref. 4). Many of these cracking tests have a significant number of uncontrolled vari-

ables that can affect cracking or crack interpretation (Ref. 9). The Varestraint tests can have solidification, liquation, and ductility-dip cracking occur in the same sample, which can make interpretation difficult and may affect the actual strain applied for DDC. Additionally, calculating the cracking temperature requires precise temperature gradient knowledge and even with skilled interpretation, it can lead to errors. Since cracking susceptibility is dependant upon the grain boundary orientation relative to the applied strain (Refs. 3, 20), all of the above tests except the STF and double spot Varestraint are sensitive to the base

material microstructure as well as the location and orientation that the samples are removed. While all of these tests have advantages and disadvantages, the authors feel that the STF test offers the greatest flexibility for evaluating the effect of applied strain and temperature on cracking susceptibility.

The Gleeble-based STF test was developed at The Ohio State University in 2002 to differentiate the DDC susceptibility of a variety of alloys and microstructures at different temperatures and strains (Ref. 19). Samples are heated to the testing temperature and strained a fixed amount. The use of the term “fracture” in the name refers to the formation of cracks (i.e., samples are strained a fixed amount and then examined for cracks). The Gleeble approach allows for precise control of temperature and strain during both STF testing and thermal processing so that each test specimen evaluates if cracking occurs at a given temperature and strain. Since the temperature is essentially uniform across the gauge section, there are no temperature gradient effects and the strain is applied at a fixed temperature. The STF test can evaluate the on-heating and on-cooling temperature range over which the ductility-dip phenomenon is observed in a material. However, in weldments it is unclear at what temperature the strain reaches sufficient levels for cracking to occur and, as such, it is not entirely clear which STF data are most relevant (Ref. 6).

Table 1 — All Weld Metal Compositions of Commercial Heats Tested FM-52, FM-52M, and Alloy 690 Base Plate (wt-%)

	FM-52 Heat NX9277	FM-52M Heat EXOA51P	Alloy 690 Plate
Ni	60.12	60.37	61.06
Cr	29.09	30.04	26.67
Fe	8.88	8.42	9.20
Nb + Ta	0.02	0.85	0.01
C	0.026	0.020	0.017
Mn	0.25	0.81	0.17
S	0.0037	0.001	0.001
P	0.0044	0.004	0.004
Si	0.17	0.03	0.06
Cu	0.011	0.02	0.02
Al	0.71	0.10	0.29
Ti	0.50	0.21	0.16
Mo	0.05	0.02	0.02
Co	—	0.007	0.009
B	—	0.004	0.001
Zr	—	0.015	—

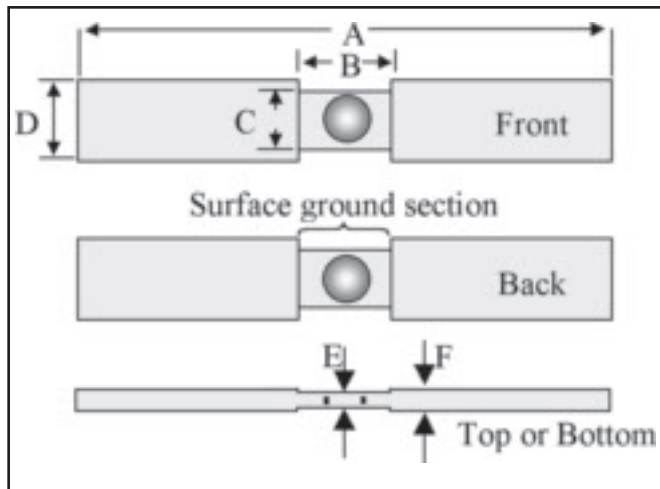


Fig. 3 — Final STF sample geometry showing dimensions and spot weld location. A = 12.7 cm (5 in.), B = 19 mm (0.75 in.), C = 15.3 mm (0.6 in.), D = 19 mm (0.75 in.), E = nominally 5.6 mm (0.22 in.), F = 6.4 mm (0.25 in.). Gauge marks were made on the top and bottom of the sample with a nominal spacing of 4 mm.

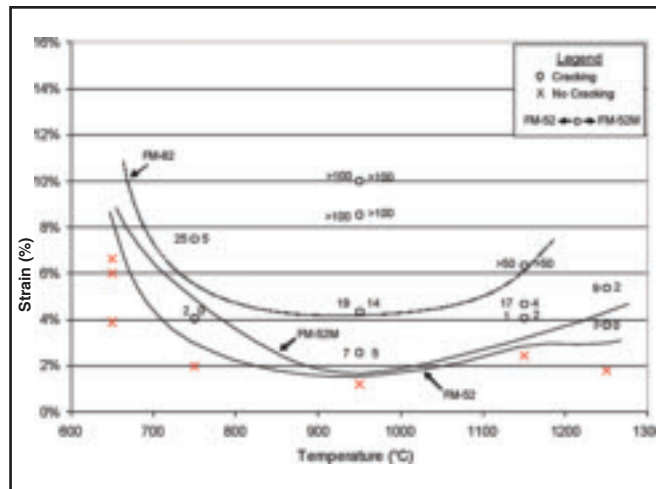


Fig. 4 — Temperature-strain curve (strain to form cracks) for FM-52 (NX9277) and FM-52M (heat EX0A51P) with results from FM-82 (heat YN7355) (Ref. 20) for comparison. An "x" represents a tested sample with no cracking and "o" a sample with cracking. The number to the left or right of the circle represents the number of cracks in FM-52 and FM-52M, respectively.

Strain-to-fracture tests have been performed on a variety of Ni-based wrought materials and filler metals and provide a good data set for comparison with the current work (Refs. 4, 11, 19, 20).

For the STF test, the DDC susceptibility of a material is evaluated by the magnitude of the ductility-dip temperature range (DTR), the threshold strain for cracking, and the transition to gross cracking. The threshold strain is defined as the maximum strain achievable before cracking occurs. The transition to gross cracking was introduced to differentiate among materials with similar threshold strains, but clear differences in cracking above the threshold (i.e., the strain level at which the cracks begin to join together, beyond which accurately counting cracks becomes difficult).

Experimental Procedures

Materials

A series of experiments was performed to investigate the effect of composition on the DDC susceptibility of Ni-based filler metals and commercially pure nickel plate. First, a heat of commercially available FM-52 (NX9277) and FM-52M (EX0A51P) was evaluated to compare the relative cracking resistance of the two alloys.

Subsequently, eight experimental FM-52M and FM-52M-like alloys were evaluated and designated A through H. Material A was a FM-152M filler metal; a SMAW electrode that is comparable to FM-52M. The remaining alloys were 0.045-in.-diameter GMAW welding wires; B, C, and G were FM-52M, E and F were

FM-72 with low and ultralow sulfur, D and H were FM-52M-like composition and additions of Nb and Mo. Filler metal 72 (FM-72) (AWS A5.14 ERNiCr-4) is often used for weld overlays of superheater tubing in power boilers to provide resistance to high-temperature corrosion.

Additionally, commercially pure Nickel 200 (99.6%) was selected for testing to evaluate a more simple alloy system to develop a fundamental understanding of DDC with fewer complex compositional interactions. The compositions of the commercial heats and the experimental alloys tested are listed in Tables 1, 2, and 3, respectively.

Sample Preparation

Two different preparation methods were used to make the STF samples. To compare the commercial consumables listed in Table 1, a preparation method (Method 1) was developed such that two different filler metal compositions could be tested in a single STF sample — Fig. 1. This preparation method allowed both

Table 2 — All Weld Metal Compositions of the Eight Experimental Alloys (A-H) (wt-%)

	Mat. A FM-152M	Mat. B FM-52M	Mat. C FM-52M	Mat. D (N/A)	Mat. E FM-72	Mat. F FM-72	Mat. G FM-52M	Mat. H (N/A)
Ni	57.2	59.54	60.38	55.5	55.90	55.87	60.14	53.87
Cr	28.68	30.06	29.5	29.6	43.33	43.09	29.53	30.18
Fe	8.75	8.22	8.04	9.0	0.08	0.27	8.33	8.2
Nb	1.53	0.83	0.82	1.0	—	—	0.78	2.48
C	0.03	0.02	0.03	0.02	0.01	0.020	0.014	0.021
Mn	3.16	0.80	0.77	0.68	<0.01	0.01	0.68	0.8
S	0.008	0.001	0.001	0.001	0.0005	0.001	0.0007	0.001
P	0.008	0.003	0.004	0.015	0.001	0.002	0.004	0.004
Si	0.3	0.09	0.12	0.03	0.03	0.03	0.12	0.2
Cu	0.04	0.02	0.01	<0.05	<0.01	<0.01	0.03	—
Al	0.04	0.11	0.12	0.05	—	—	0.13	0.04
Ti	0.07	0.22	0.19	0.20	0.55	0.53	0.19	0.2
Mo	—	—	—	4.0	—	—	0.02	4
B	0.002	0.003	0.001	0.004	—	—	0.001	0.001
Zr	0.003	0.01	0.008	0.006	—	—	0.0006	0.007

Table 3 — Nominal and Actual Compositions of the Ni 200 Plate

	Nickel 200 Specifications	Nickel 200 Heat N13T8A12
Ni (+Co)	99.0 min	99.54
Cu	0.25 max	0.07
Fe	0.40 max	0.10
Mn	0.35 max	0.20
C	0.15 max	0.06
Si	0.35 max	0.03
S	0.01 max	<0.001

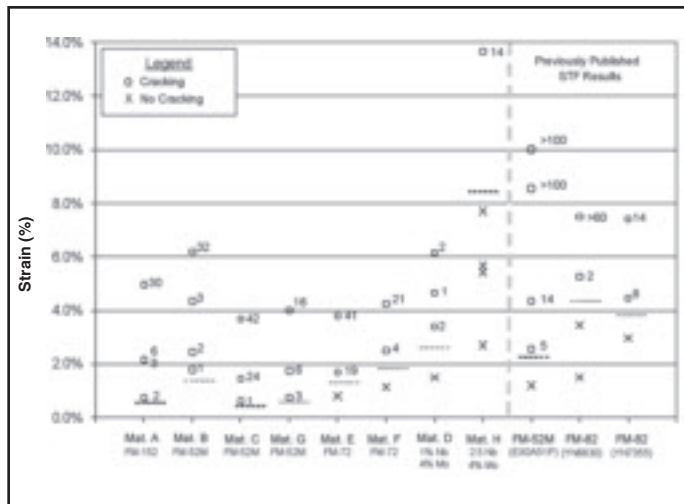


Fig. 5 — STF test results (strain to form cracks) for baseline testing at 950°C for experimental FM-52M and FM-72 compositions (A through H) along with the results of previously tested FM-52M and FM-82 (Ref. 20). An “x” represents a tested sample with no cracking and “o” a sample with cracking. The number next to the circle is the number of cracks found. For each material, the dashed line approximates the threshold strain (strain at which cracks initiate).

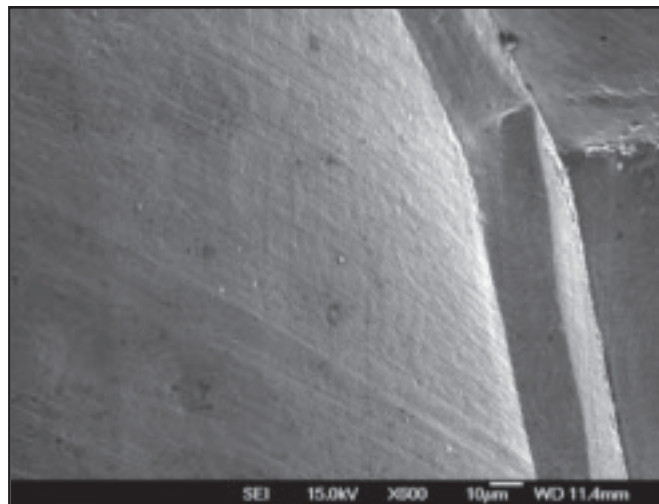


Fig. 6 — Fracture surface of Ni 200 STF sample tested at 950°C showing the intersection of several grains with macroscopically flat intergranular fractures and evidence of crystallographic slip. The grain boundaries are relatively clean and free of carbides.

filler metals to be tested at the same temperature and strain (in a single sample). A 0.25-in.- (6.4-mm-) thick plate of Alloy 690 was machined with 0.75 in. (19 mm) wide by 0.083 in. (2.1 mm) deep grooves with 45-deg beveled edges on opposite sides of the plate. Alternating passes of FM-52 and FM-52M (Table 1) were made on opposite sides of the plate (distortion control) to fill in the machined grooves with weld metal. The GTAW process with cold wire feed (CWF) was used to deposit

the filler metal. Three layers of weld metal beads (3 or 4 per layer) were required to completely fill the grooves and dilution of the top layer of weld metal by Alloy 690 base metal was estimated to be 10% (using metallographic evaluation of cross section). Any weld reinforcement was ground flush, radiographed, and standard STF sample blanks were laser cut from the welded plates so that the location of the FM-52 and FM-52M welds corresponded with the reduced center section of the STF sample. The final sample dimensions are provided in Fig. 3.

The experimental consumables listed in Table 2 were evaluated with a more standard preparation method (Method 2) where samples were prepared so that a single composition could be tested with each sample — Fig. 2. Two 0.75-in.- (19-mm-) thick plates of Alloy 690 had 30-deg beveled faces machined so they formed a 60-deg included angle V-groove. The weld metal was deposited to completely fill the groove (Fig. 2), any weld reinforcement was ground flush and the samples were radiographed. Grooves 0.75 in. (19 mm) wide were machined on the top and bottom of the sample to make the reduced

center section. The plate was cut into 0.25-in. (6.4-mm) pieces with a band saw and squared with a mill into standard STF sample blanks with dimensions shown in Fig. 3. These samples were prepared by the Special Metals Welding Products Co. (Ref. 21).

For the commercially pure Ni 200 samples, STF sample blanks were laser cut from a 0.25-in. (6.4-mm) plate using the standard procedure for wrought materials (Ref. 19). The final sample dimensions are provided in Fig. 3.

The starting microstructure (e.g., grain size, boundary morphology, carbide type, and distribution) in a STF sample is known to have a significant effect on the DDC susceptibility (Refs. 3, 6, 14, 20, 22). Since each of the above sample preparation methods impart different thermal histories and chemistry variations in the samples due to the multipass welding techniques applied, autogenous gas tungsten arc spot welds were made on both the front and back faces of each reduced section of sample before STF testing (Fig. 3) to create a reproducible microstructure (Refs. 11, 19).

The welding procedures used for the GTA spot welds are listed in Table 4. These welds were made in a copper fixture to provide consistent and controlled heat flow from the sample. One of the spot weld variables is the downslope time and is defined as the time for the current to ramp down from the peak current of 140 A to 20 A. All of the previous STF tests (Ref. 19) and the majority of the samples tested during this investigation were performed with a 12.7-s

Table 4 — Welding Procedures for STF Spot Welds Using GTAW

	Value	Time
Voltage	12.5 V	
Preflow	20 ft ³ /h	10 s
Start Level	20 A	0.1 s
Initial Slope		5 s
Weld	140 A	20 s
Downslope	12.7 s (standard) 5 s (where noted)	
Final Level	20 A	0.1 s
Postflow	20 ft ³ /h	15 s
Shielding Gas	20 ft ³ /h Argon (99.998%)	

Table 5 — Microstructural Variation in Material B Comparing a 5- and 12.7-s Downslope Spot Weld

Downslope Time	Avg. Subgrain Spacing	MC-Type Carbides	
		Optical Area Fraction	SEM Area Fraction
5 s	16.4 µm	1.30%	0.26%
12.7 s	20.4 µm	0.80%	0.19%
Difference	24%	62%	37%

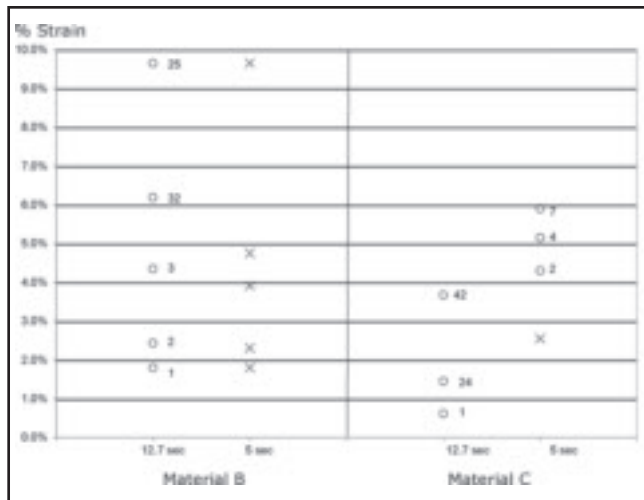


Fig. 7 — Results of 5- and 12.7-s downslope in spot welds of B and C tested at 950°C. An “x” represents a tested sample with no cracking and “o” a sample with cracking. The number next to the circle is the number of cracks found.

downslope time. However, initial welds in the Ni 200 plate with the 12.7-s downslope prewelds resulted in extensive cracking that was only avoided by reducing the downslope to 5 s. As a result of this finding, all the Ni 200 samples and select Ni-Cr-Fe filler metal STF tests were run with a downslope time of 5 s.

Following the placement of the spot welds on the sample, the front and back faces of the reduced center section were surface ground (equivalent to at least 320 grit SiC grinding paper) to remove any surface roughness or oxidation caused by welding and to allow for easier crack detection after testing (Fig. 3). In contrast to previous STF testing reported by the authors, the samples were not pre-etched prior to STF testing as this was found to be an unnecessary sample preparation step, and it had no detectible effect on cracking (Ref. 4).

Gauge marks with a spacing of 4 mm (0.157 in.) were placed on the bottom and top of each sample (Fig. 3) with two square indentions made with a modified punch. The initial (and final) gauge spacing was measured between the punch marks at 100× magnification on a stage controlled by a digital micrometer. This technique allows for precise and consistent strain measurement in the gauge section of the sample after testing.

STF Testing Procedure and Analysis

The STF testing was performed using a Gleeble 3800 utilizing a hot zone L-strain gauge to measure deformation across the gauge section of the STF sample. The L-strain gauge was seated into the square indentions used to mark the gauge and allowed for real-time information on sample deformation to be used

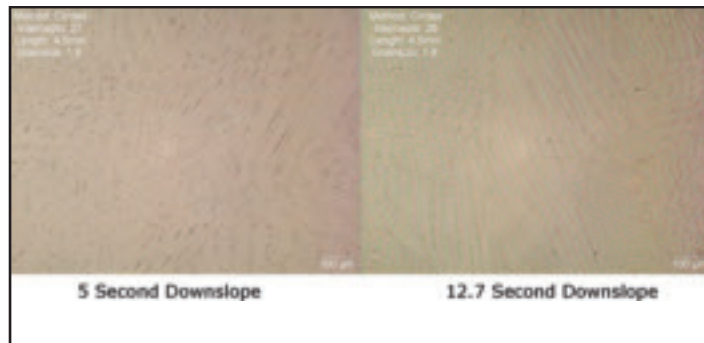


Fig. 8 — Typical optical photomicrographs of B made with 5- and 12.7-s downslope spot welds. The grain size did not vary significantly, but the 5-s downslope weld had a greater area fraction of MC-type carbides and a finer subgrain size.

for feedback control. A K-type control thermocouple was used to measure temperature.

Prepared samples were mounted in stainless steel hot jaws with knurled tool steel grips in the Gleeble with a jaw (or free-span) spacing of 2 in. (50.8 mm). A rough vacuum (10^{-2} torr) was applied to the chamber of the Gleeble and then back purged with argon (99.998% Ar). This was repeated to ensure minimal oxidation during testing.

For this work, samples were only tested on-heating to minimize the number of testing variables (peak temperature, time at temperature, cooling rate, etc.). The Gleeble was programmed to heat the sample to the test temperature at 100°C/s and hold at the test temperature for 10 s to allow the temperature to stabilize within the gauge section. The sample was then strained by moving the jaws of the Gleeble at a constant rate of 0.06 cm/s (0.024 in./s) until the L-strain gauge reached a predetermined value indicating that the sample had been strained to the desired level. Details of the Gleeble program are available elsewhere (Ref. 4). Once the desired strain was obtained, the heating was turned off and the sample was allowed to free cool to room temperature under a zero load condition (using load control to compensate for thermal contraction). By cooling under a zero load condition, any cracking that occurred could be attributed to straining at the test temperature rather than strain that accumulated during cooling.

The tested samples were evaluated for cracking using a stereo microscope at magnifications from 10 to 30×. The final gauge spacing was measured on the top and bottom of the sample, and the actual plastic strain was calculated as $\Delta L/L_0$. The average strain (top and bottom) and the test temperature were plotted on a temperature-strain curve. The threshold

strain and the transition to gross cracking were used to evaluate the DDC susceptibility of the tested materials. The threshold strain is defined as the minimum strain (over the DDC temperature range) at which DDC occurs. The transition to gross (massive) cracking was considered to have occurred when the ability to accurately count the number of cracks in one spot weld became difficult. The transition to gross cracking is typically observed when the number of cracks in a spot weld exceeds approximately 20 cracks. However, in highly susceptible materials where cracks begin joining together at low strains, the transition to gross cracking is not as easy to define using simply a fixed number of cracks. Rather, it can be quantified by calculating the rate of increase in the number of cracks from one sample to the next and occurs when approximately 10 cracks per percent strain is reached.

Solidification Microstructure Analysis

The as-welded spot weld microstructure of both downslope conditions (12.7 and 5 s) were evaluated with SEM and optical microscopy. SEM images at 500× magnification and optical images at 100× magnifications were analyzed to determine the grain size, dendrite arm spacing, and area fraction of MC-type carbides. For each downslope condition, grain size and precipitate area fraction measurement were conducted on multiple images that traversed the spot weld. *PAX-it* (Ref. 23) was used to measure the ASTM grain size, and *ImageTool* (Ref. 24) was used to quantify the area fraction of MC-type carbides. Since the solidification subgrain (cell and dendrite) microstructure varied across the spot weld, the dendrite arm spacing was measured at a distance of 1.5 mm from the edge of the spot for consistency. The distance across multiple dendrites was measured, and the average was calculated with a minimum of 35

measurements.

The cooling rate in spot welds for different (weld current) downslope times was investigated with thermocouple measurements. A 1.75-mm- (0.069-in.-) diameter hole was machined in the back side of the sample to within 1.5 mm (0.06 in.) of the front surface (located just inside the spot weld fusion zone). The hole was located so that it would be approximately 1.5 mm (0.06 in.) from the spot weld edge for comparison with the metallographic analysis. A thermocouple with a 1.5-mm (0.06-in.) ceramic insulator was inserted in the hole and a spot weld was made on the front face of the sample. The results of the 5- and 12.7-s downslope spot welds were compared to understand the thermal histories and resulting microstructures.

Results and Discussion

FM-52 and FM-52M (Method 1)

Samples of FM-52 and FM-52M (Table 1) were made using sample preparation Method 1 (Fig. 1) and STF tested from 650° to 1250°C with the results shown in Fig. 4. The compositions of the two alloys are similar with the exception of B, Nb, and Zr additions to FM-52M. Samples that did not crack were marked with an "x" and samples of either FM-52 or FM-52M that cracked were marked with a circle. The actual number of cracks observed in each sample is included next to each point (FM-52 and FM-52M are to the left and right, respectively) to further aid in the interpretation of the results. A curved line was drawn separating cracked and crack-free samples, which represent the threshold strain required for DDC across the entire temperature range. While a more precise determination of the threshold strain can be determined if additional samples are run, cracking trends are observed in STF data and a good approximation of the threshold strain estimated when samples are 1–2% apart.

Over the temperature range evaluated, the minimum in the threshold strain curve for both materials occurred at approximately 950°C and 2% strain with FM-52M demonstrating a slightly higher resistance (fewer cracks observed in all but one sample). The temperature where the minimum threshold strain was observed (950°C) is consistent with STF testing of other materials (usually occurring somewhere between 900° and 1000°C) (Ref. 19). Previous results from STF testing of FM-82 (Ref. 20) are superimposed on Fig. 4 for reference.

With the exception of one sample (1150°C, 4.1%), FM-52M consistently had fewer total cracks than FM-52 including two samples where cracks were only found

in FM-52 (750°C, 4.1%, and 1250°C, 3.8%). In these two samples where cracking did not occur in FM-52M, evidence of grain boundary sliding and localized strain around the boundaries was observed indicating the sample was on the verge of cracking (Ref. 4). As the strain increased, the cracking susceptibility difference between the filler metals became less obvious.

These results are consistent with the heat-to-heat variation in DDC resistance reported in the literature (Ref. 20). Since DDC susceptibility is sensitive to small changes in composition (and susceptibility), these results should be assumed to be a heat-to-heat comparison and not a general representation of these two alloys. Since the current understanding of the DDC mechanism does not include a robust understanding of the overall effect of composition, testing of individual heats for DDC susceptibility should be considered for critical applications.

Experimental Ni-Cr-Fe Alloys (Method 2)

Previous testing (Refs. 19, 20) has shown that the STF ductility minimum for most nickel alloys occurs between 850° and 1050°C and gross cracking is typically observed first in this temperature range (i.e., at lower strains than other temperatures). Based on this observation, STF testing was performed at a single temperature of 950°C to assess susceptibility of a large number of filler metal compositions using only a limited number of samples. Based on previous experience with the STF test, it was felt that this approach was appropriate for screening multiple compositions. The results of STF testing at 950°C are shown in Fig. 5 with previously reported STF results for FM-52M and FM-82 compositions plotted for reference.

The threshold strains for A–G varied between 1 and 3% while that for H was significantly higher at approximately 8%. Accordingly, the transition to gross cracking for A–G varied between 4 and 7% while for H it was >14%. The composition of B and C were of particular interest because while their compositions were quite similar (except for a small variation in boron), they exhibited significantly different resistance to DDC. Both B and C had a relatively low threshold strain at 950°C (<1.5%), but the additional strain required to transition to gross cracking was much higher in B (>5%) vs. in C (1.5%). Thus, although the threshold strains are similar, testing at higher strains suggests that C is much more susceptible to DDC than B.

Based upon this screening, the DDC resistance of the FM-52M (B, C, G) and FM-72 (E, F) alloys is lower than that of FM-82 while the FM-52M-type composi-

tion with the addition of 4% Mo and 2.5% Nb (H) was the highest. Of the 30% Cr Ni-based filler metals tested to date, the combined additions of Nb and Mo exhibited the best DDC resistance at 950°C.

E and F are heats of FM-72 that were evaluated because of their low sulfur content. Since sulfur has been identified by other investigations (Refs. 5, 15, 20, 25) to be contributory to DDC, these heats were of interest. The sulfur levels found in F would, under most conditions, be considered low while the ultralow sulfur level found in E required additional processing. The number of DDC cracks that were observed in F and the ultralow sulfur E could not have been solely predicted based on the level of sulfur. Several factors do complicate the interpretation of this result including the higher Cr (Ref. 26) in FM-72 and lower Mn (Ref. 15). This result does not dismiss the effect of sulfur; instead, it highlights the complexity of the DDC mechanism and the combined effect of several factors. While sulfur has been shown to increase DDC (and solidification cracking) (Refs. 5, 20, 25, 27), it may also affect boundary mobility and materials with extremely low impurity content have been found susceptible to DDC (Ref. 4). An optimum sulfur value likely exists where positive boundary drag effects balance a negative embrittling effect.

D and H (FM-52M-type) with 4% molybdenum and 1 and 2.5% niobium, respectively, exhibited improved cracking resistance when compared to the other six materials tested in this investigation. D had a threshold strain and gross cracking strain of 2.5 and >6%, respectively, which is high compared to the other alloys with 1% niobium. H had a threshold strain and a gross cracking strain of 8 and 14%, respectively, which approaches that of materials that are quite resistant to DDC such as austenitic stainless steel weld metal containing ferrite (Refs. 19, 28).

Niobium has been proposed to be an element that improves DDC resistance by forming MC-type carbides at the end of solidification and which subsequently pin grain boundaries (Refs. 14, 15). While Ni-based alloys with 2 to 3% niobium are consistently more resistant to DDC than those with less than 1%, niobium content by itself has not been directly correlated to cracking resistance (Refs. 14, 15). The morphology, size, temperature of formation, and distribution of the MC carbides are affected by other alloying elements, and it is likely the combined effect of other elements with Nb (such as Mo) that is contributing to the overall improvement of these alloys.

Based upon the results of the initial screening, three alloys were selected for further metallurgical evaluation. H was

selected for its superior DDC resistance at 950°C. B and C were selected because of their similar compositions but differing DDC resistance. The results of this subsequent metallurgical evaluation are the subject of Part 2 of this paper.

Commercially Pure Ni 200

During the preparation of the Ni 200 samples, extensive cracking was observed at the completion spot welds made with 12.7-s downslope spot welds. It was discovered that crack-free welds were produced with a faster downslope time of 5 s, and these were subsequently STF tested in the Gleeble. Cracking occurred in all Ni 200 samples tested (all at 950°C), regardless of the strain and the extent of gross cracking prohibited a comparative crack count. Analysis of the fracture surface confirmed that the cracks were macroscopically flat intergranular fractures, consistent with other DDC cracks — Fig. 6. The lack of second phases in the alloy and the resulting large grains in the spot weld may have contributed to the extreme sensitivity to DDC observed in this alloy. Further evaluation of this alloy was not conducted due to the extent of DDC by both Type 2B (DDC in primary weld metal) and 2C (DDC in reheated weld metal) cracking (Ref. 29). The observed cracking difference from the spot weld solidification microstructure (produced through spot weld downslope time variations) was investigated further with the experimental Ni-Cr-Fe alloys.

Solidification Microstructure Effects (Downslope Time)

In standard STF testing, an autogenous spot weld was made before STF testing with a 12.7-s downslope time from 140 to 20 A is used to ensure a controlled solidification microstructure that is consistent from sample to sample. Through previous studies, this spot weld has been shown to generate a radial pattern of grain boundaries that is relatively consistent among the various materials tested (Ref. 11). To evaluate the effect of a shorter downslope time on the solidification microstructure and resultant cracking observed in Ni 200, samples of B and C were made with a 12.7- and 5-s downslope spot weld on opposite sides of the same sample. This allowed a direct comparison as the chemistry, temperature, and strain were the same for a given sample. To confirm the second spot weld did not affect the first, the spot weld sequence was made randomly. Post-test evaluation found no significant effect of the spot weld sequence on the DDC susceptibility when welding was conducted in the copper fixture, which provided a larger thermal mass.

Results of this experiment (Fig. 7)

demonstrated that reducing the current downslope time significantly decreased the cracking susceptibility (both the threshold strain and gross cracking transitions) of both B and C, although a greater improvement was observed in B. Embedded thermocouples revealed that the time required for the sample to cool from 1400° to 1150°C was 4 s for the fast downslope time and 6.8 s for the normal downslope time (Ref. 4). The cooling rate below 1150°C (approximately the nonequilibrium solidification solidus based upon JMatPro calculations) was the same for both welds because the thermal mass of the copper fixture was sufficient to overcome the difference in heat input.

Microstructural evaluations of B (Fig. 8) revealed that decreasing the downslope time from 12.7 to 5 s had little effect on the final grain size (average of ASTM 1.85 and 2.0, respectively) but reduced the subgrain size (cell and dendrite spacing) by 24%, and increased the area fraction of MC-type carbides by approximately 50% area fraction — Table 5.

The decrease in the number of MC-type carbides under the slower cooling rate condition (12.7-s downslope) was attributed to the metastable nature of these carbides. The MC-type carbides form at the end of solidification due to the segregation of Nb that promotes a terminal eutectic reaction consisting of austenite and Nb-rich MC carbide (Ref. 30). Since the MC carbides are not a stable equilibrium phase at elevated temperatures (in FM-52 or FM-52M), they begin to dissolve into the matrix with additional time at temperature (slower cooling rate). While MC-type carbides have been proposed to improve cracking resistance by limiting grain boundary migration (Ref. 20), no significant grain size differences were observed optically. The effect of small changes in the amount and morphology of MC carbide on grain boundary tortuosity and grain boundary properties is still not fully understood, but these carbides have been attributed to greater resistance to DDC in some cases (Ref. 14). It is unclear if the improved resistance is the result of the MC-type carbides, the finer substructure, or a combination of both. A series of additional heat treatments to control carbide dissolution would be required to better understand this observation.

In arc welding, heat input affects the cooling rate in a similar manner as downslope does in the STF spot welds. Therefore, any variation in cracking resistance as a result of the spot weld has potential implications on the heat input in production welds. To date, no STF testing variable has been found with greater influence on DDC susceptibility than the downslope time of the spot welds.

Conclusions

1. The FM-52M-like filler metal with 2.5% Nb and 4% Mo had significantly improved DDC resistance at 950°C relative to other 30% Cr alloys and FM-82.
2. The FM-52M experimental alloys exhibited a large variation in DDC susceptibility that could not be simply explained by the minor differences in composition.
3. For preparation of the strain-to-fracture samples, the GTA spot weld downslope time and subsequent solidification microstructure had a significant effect on the DDC susceptibility. This is the most influential STF test variable evaluated to date.
4. Commercially pure Ni 200 was found to be extremely sensitive to DDC and is the most DDC susceptible alloy tested to date with the STF test.
5. Reducing the downslope time of the GTA spot weld was found to reduce DDC susceptibility in FM-52M. The faster cooling rate through the solidification temperature range promoted a finer solidification substructure and a higher fraction of MC carbide that improved the DDC resistance of the materials.

Acknowledgments

The authors would like to thank Sam Kiser of Special Metals, and Dr. Suresh Babu, Morgan Gallagher, Ray Unocic, and Kenny Izor from The Ohio State University for their assistance and insight during the course of this investigation. Thanks also to Special Metals Welding Products Co. for supplying filler metals and sample blanks used in some of the testing. Partial financial support for project was provided by BWXT, Inc.

References

1. Kiser, S. D., et al. 2005. Nickel alloy welding requirements for nuclear service. *Focus on Nuclear Power Generation 2005*.
2. Lin, W., and Cola, M. J. 1997. Weldability of Inconel filler metal 52. 78th American Welding Society Annual Meeting, Abstracts of Papers, April 13–17, Los Angeles, Calif.
3. Kikel, J. M., and Parker, D. M. 1998. Ductility-dip cracking susceptibility of filler metal 52 and Alloy 690. *Trends in Welding Research*, June 1–5, Pine Mountain, Ga.
4. Nissley, N. E. 2006. Intermediate temperature grain boundary embrittlement in nickel-base weld metals. Columbus, Ohio: The Ohio State University, p. 204, www.ohiolink.edu/etd/view.cgi?acc_num=osu1156949345.
5. Nishimoto, K., Saida, K., and Okauchi, H. 2006. Microcracking in multipass weld metal of Alloy 690, Part 1 — Microcracking susceptibility in reheated weld metal. *Science and Technology of Welding and Joining* 11(4): 455–461.
6. Ramirez, A. J., and Lippold, J. C. 2004.

High temperature behavior of Ni-base weld metal. I. Ductility and microstructural characterization. *Materials Science & Engineering A* 380(1-2).

7. Lippold, J. C., Clark, W. A. T., and Tumuluru, M. 1992. An investigation of weld metal interfaces. *The Metal Science of Joining*, published by The Metals, Minerals and Materials Society: 141-146.

8. Gooch, T. G., and Honeycombe, J. 1975. Microcracking in fully austenitic stainless steel weld metal. *Metals Construct.* 7(3): 146-148.

9. Yeniscavich, W. 1966. A correlation of Ni-Cr-Fe alloy weld metal fissuring with hot ductility behavior. *Welding Journal* 45(8): 344-s to 356-s and 384-s.

10. Newell. 1933. The performance of 18-8 at high temperature. *Book of Stainless Steel*. Ed. E. E. Thum. The American Society for Steel Treating, p. 364.

11. Nissley, N. E. 2002. Development of the strain-to-fracture test to study ductility-dip cracking in austenitic alloys. *Welding Engineering*. Columbus, Ohio: The Ohio State University, p. xv, 104 leaves.

12. Lippold, J. C., and Ramirez, A. J. July 2004. Insight into the mechanism of ductility dip cracking. *IIW-IX-2123-04*. Osaka, Japan.

13. Zhang, Y. C., Nakagaw, H., and Matsuda, R. 1985. Weldability of Fe-36%Ni alloy (Report V). *Transactions of JWRI* 14(2): 119-124.

14. Collins, M. G., Ramirez, A. J., and Lippold, J. C. 2004. An investigation of ductility-dip cracking in nickel-based weld metals — Part III. *Welding Journal* 83(2): 39-s to 49-s.

15. Ramirez, A. J., and Lippold, J. C. 2004. High temperature behavior of Ni-base weld metal. II. Insight into the mechanism for ductility dip cracking. *Materials Science & Engineering A* 380(1-2).

16. Haddrill, D. M., and Baker, R. G. 1965. Microcracking in austenitic weld metal. *British Welding Journal* 12(9).

17. Blum, B. S., and Witt, R. H. 1963. Heat-affected zone cracking in A-286 weldments. *Welding Journal* 42(8): 365-s to 370-s.

18. Honeycombe, J., and Gooch, T. G. 1970. Microcracking in fully austenitic stainless steel weld metal. *Metal Construction & British Welding Journal* 2(9): 375-380.

19. Nissley, N. E., et al. 2002. Development of the strain-to-fracture test for evaluating ductility-dip cracking in austenitic stainless steels and Ni-base alloys. *Welding in the World* 46(7/8): 32-40.

20. Collins, M. G., and Lippold, J. C. 2003. An investigation of ductility dip cracking in nickel-based filler metals — Part I. *Welding Journal* 82(10): 288-s to 295-s.

21. Special Metals Welding Products Co. 2006 cited. Visit www.specialmetals.com.

22. Ramirez, A. J., and Lippold, J. C. March 2004. New insight into the mechanism of ductility dip cracking in Ni-base weld metals. *1st International Workshop, Hot Cracking Phenomena in Welds*, 19-41. Berlin: Springer-Verlag.

23. Midwest Information Systems, I.M. PAX-it image management and image analysis software. 2006 cited. Visit www.paxit.com.

24. Wilcox, C. D., et al. *ImageTool*. 2002 cited. Visit ddsdx.uthscsa.edu/dig/itdesc.html.

25. Nishimoto, K., Mori, H., and Hongoh, S. 1999. Effect of sulfur and thermal cycles on re-heat cracking susceptibility in multi-pass weld metal of Fe-36% Ni alloy. *IIW Doc. IX-1934-99*.

26. Yzoung, G. A., et al. 2008. The mechanism of ductility dip cracking in nickel-chromium alloys. *Welding Journal* 87(2): 31-s.

27. Collins, M. G. 2002. An investigation of ductility dip cracking in nickel-base filler materials. The Ohio State University, p. xix, 240 leaves.

28. Lippold, J. C., and Nissley, N. E. 2008. Ductility dip cracking in high-Cr Ni-base filler metals. *International Workshop on Hot Cracking*. Berlin: Springer-Verlag.

29. Hemsworth, B., Boniszewski, T., and Eaton, N. F. 1969. Classification and definition of high temperature welding cracks in alloys. *Metal Construction & British Welding Journal*: 5-16.

30. DuPont, J. N., Robino, C. V., and Marder, A. R. 1998. Modeling solute redistribution and microstructural development in fusion welds of Nb-bearing superalloys. *Acta Materialia* 46(13): 4781-4790.

Call for Papers

**1st International Conference on Welding Technologies '09
June 11-13, 2009
Gazi University, Ankara, Turkey**

Abstract submission deadline: October 25, 2008

The following areas and topics are proposed as a guide for papers, but authors are not limited to these topics.

- Welding Metallurgy
- Mechanical Properties
- Welding Processes
- Welding Defects and Testing
- Industrial Applications
- Modeling/Simulation
- Microjoining
- Education and Training on Welding
- Automation
- Advanced Welding Technologies
- Welding Design
- Health and Environment

Authors are invited to submit abstracts of papers for presentation in the conference technical program. Abstracts must be 100-150 words and should not contain figures or tables. Abstracts should include title, name and full address of the author, and name and address of coauthors, if any. Authors should indicate whether they would prefer to present their papers orally or as a poster. Submit abstracts online at icwet09@gazi.edu.tr. For additional information, visit the conference Web site at www.icwet09.org.